Journal of Materials Chemistry A

Accepted Manuscript

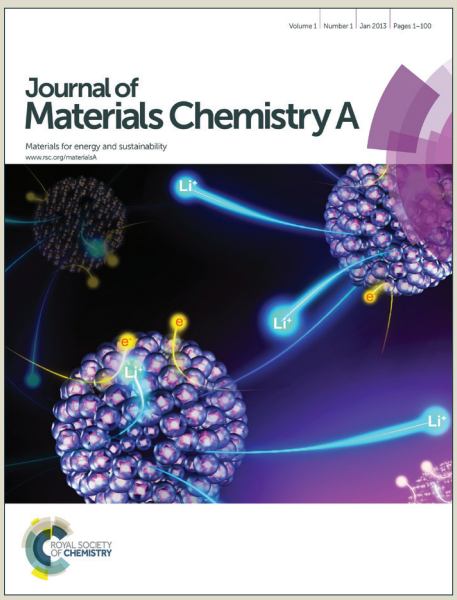

ROYAL SOCIETY OF CHEMISTRY

www.rsc.org/materialsA

Journal Name

RSCPublishing

ARTICLE

Exceptional Pseudocapacitive Properties from Hierarchical NiO Ultrafine Nanowires Grown on Mesoporous NiO Nanosheets

Cite this: DOI: 10.1039/x0xx00000x

Received 00th January 2012,
Accepted 00th January 2012

DOI: 10.1039/x0xx00000x

www.rsc.org/

Lei An[a], Kaibing Xu[a], Wenyao Li[a,b], Qian Liu[a], Bo Li[a], Rujia Zou[a,c,*], Zhigang Chen[a] and Junqing Hu[a,*]

Hierarchical NiO ultrafine nanowires grown on mesoporous NiO nanosheets with Ni foam as substrate synthesized by a facile and effective hydrothermal method showed exceptionally high specific capacitance (1349 F g^{-1} at a current density of 5 A g^{-1}), good rate performance (~ 58% retention of the initial capacitance from 3 A g^{-1} to 50 A g^{-1}) and superior electrochemical cycling stability (~ 87% retention after 2000 cycles). The remarkable electrochemical performance can make the unique hierarchical NiO nanosheets/nanowires to be a perspective electrode material for electrochemical energy storage applications.

Introduction

With the fast-increasing demand for high-power applications such as portable systems and hybrid electric vehicles, the research on electrochemical capacitors (ECs), also known as supercapacitors, has drawn tremendous attention owing to numerous irreplaceable properties like high specific capacitance, fast charge and discharge rate, good rate capability and long cycle lifetime.[1-4] It is well known that electrode materials play a vital role in the development of high performance supercapacitors. Up to now, typical transition metal oxides/hydroxides, such as RuO_2,[5] $Ni(OH)_2$,[6] NiO,[7,8], Co_3O_4,[9,10] and $Co(OH)_2$,[11,12] which could provide a variety of oxidation states for efficient redox charge transfer, have been widely investigated as advanced electrode materials. Among these candidates, NiO is believed to be a fascinating pseudocapacitive electrode material due to its high theoretical capacitance (2584 F g^{-1}), environmental friendliness, low cost, excellent pseudocapacitive properties and good corrosion stability in alkaline solutions.[13-16] Many reports are available on the synthesis and pseudocapacitive properties of NiO electrode material with various nano/microstructures, such as NiO hollow nanospheres (612.5 F g^{-1} at 0.5 A g^{-1}),[17] flower-shaped NiO (381 F g^{-1} at 1 A g^{-1}),[14] NiO nanotubes (405 F g^{-1} at 0.5 A g^{-1}),[18] mesoporous NiO network-like hierarchical microspheres (555 F g^{-1} at 2 A g^{-1})[19] and so forth. Unfortunately, in these cases above the observed specific capacitances are still far below the theoretical values, especially at high rates, as these active materials possess poor electric conductivity and fail to support a fast electron transport required at high rates. The charge transfer kinetics to fully utilize the redox reactions for supercapacitors can be significantly enhanced by rational designing additive/binder-free electrode nanostructures which can avoid the conventional tedious preparation process and allow for more efficient mass and charge exchange, resulting in exceptional pseudocapacitive performance.[20-22]

It is well accepted that both morphologies and microstructures play essential roles in optimizing the performance of supercapacitors. Among various nano/microstructures, one-dimensional nanostructured materials have been intensely investigated due to their short diffusion pathways for electrons and ions, resulting in high charge/discharge rates during electrochemical energy storage.[23,24] Until now, one-dimensional nanostructures with a larger diameter of tens of nanometers, normally including nanowires,[25,26] nanofibers,[27] nanorods,[28] and nanobelts,[29] have been fabricated through diverse approaches. However, marginally larger dimension may greatly reduce the electroactive sites for the electrode materials, resulting in lower pseudocapacitive properties. Hence, ultrafine nanostructures with a diameter below 10 nm have gained great interest for high-performance supercapacitors. Moreover, complex hierarchical nanostructures with large surface areas and more electroactive sites of the outer branches have been demonstrated to improve the utilization of active material for high electrochemical performance.[10,21,30-32] Although hierarchical structures have been synthesized from many metal oxides, the controllable synthesis of NiO material with desirable hierarchical architecture possessing an ultrafine nanostructure and predominant electrochemical performance still remains a great challenge.

In this work, we utilized a facile, effective, and low-cost hydrothermal method to prepare hierarchical structures of NiO ultrafine nanowires grown on mesoporous NiO nanosheets with Ni foam as substrate. Within as-formed hierarchical structures, NiO nanosheets firstly uniformly grew on the Ni foam as a secondary microstructure, forming a 3D porous framework, and then NiO ultrafine nanowires interconnected with each other are rooted on the nanosheets, exhibiting a unique porous

hierarchical feature with suitable intervals among adjoining nanostructures. The hierarchical NiO nanosheets/nanowires delivered an ultrahigh specific capacitance of 1349 F g^{-1} at 5 A g^{-1}, which is superior to 1130 F g^{-1} of the NiO nanosheet arrays at the same current density. Furthermore, this electrode material exhibited a high specific capacitance (867 F g^{-1}) at the current density as high as 50 A g^{-1}, a good rate performance (~58% retention of the initial capacitance from 3 A g^{-1} to 50 A g^{-1}) and a high electrochemical stability (~ 87% retention after 2000 cycles). Such an excellent electrochemical performance can make the synthesized hierarchical NiO nanowires/nanosheets to be one of the perspective electrode materials for electrochemical energy storage applications.

Experimental Characterization

Synthesis

All the chemicals were of analytical grade and used without further purification. Firstly, a piece of Ni foam (~ 4 cm × 1 cm) was carefully cleaned with 6 M HCl solution in an ultrasound bath for 10 min to remove NiO layer on the surface, and then rinsed with deionized water and absolute ethanol for several times till neutral. Secondly, 0.3 g $Ni(NO_3)_2$•$6H_2O$ and 1.0 g urea were dissolved in 48 mL deionized water to form a homogeneous absinthe-green solution. The solution and the pre-treated Ni foam were transferred into a 60 mL Teflon-lined stainless-steel autoclave, which was sealed and maintained at 120 ℃ for 2 h (for the growth of mesoporous NiO nanosheet arrays), 120 ℃ for 6 h (for the growth of NiO nanosheets/nanowires). After being cooled down to room temperature, the products were collected and washed with deionized water and absolute ethanol, then vacuum dried at 50 ℃ for 4 h. Lastly, the products were calcined at 350 ℃ in a normal nitrogen atmosphere with a ramping rate of 2 ℃ min^{-1} for 2 h.

Characterization

X-ray diffraction was carried out with D/max-2550 PC X-ray diffractometer (XRD; Rigaku, Cu-Kα radiation), the morphology of as-prepared products was examined by a scanning electron microscope (SEM; S-4800) and a transmission electron microscope (TEM; JEM-2010F) equipped with an energy dispersive X-ray spectrometer (EDX). The surface area, pore size, and pore-size distribution of the products were determined by Brunauer-Emmett-Teller (BET) nitrogen adsorption-desorption and Barrett-Joyner-Halenda (BJH) methods (Micromeritics, ASAP2020). The mass of electrode materials was weighed on an XS analytical balance (Mettler Toledo; δ = 0.01 mg).

Electrochemical measurement

Electrochemical measurements were performed on an Autolab Electrochemical Workstation (PGSTAT302N) using a three electrode electrochemical cell and 6 M KOH as the electrolyte. The Ni-foam-supported electroactive materials (~ 1 cm × 1 cm, ~ 1.01 mg cm^{-2}) were used directly as the working electrode. A saturated calomel electrode (SCE) was used as the reference electrode and a platinum (Pt) sheet electrode was used as the counter electrode. All potentials were referred to the reference electrode. The specific capacitance and current density were calculated based on the mass of these electroactive materials.

Results and discussion

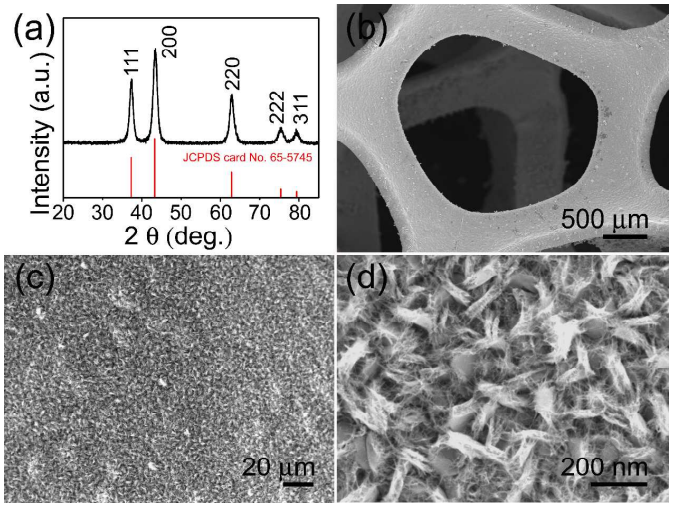

Fig. 1 (a) XRD pattern of the hierarchical NiO nanosheets/nanowires scraped off from the Ni foam. (b-d) different magnification SEM images of the hierarchical NiO nanosheets/nanowires on Ni foam.

To minimize the impact of the Ni foam substrate, X-ray diffraction (XRD) measurements were conducted from powder samples scraped off from the Ni substrates. As shown in Fig. 1a, all diffraction peaks can be unambiguously assigned to cubic phase NiO (JCPDS card No.: 65-5745). It implies that a calcined temperature at 350 °C is sufficient to convert the precursor to pure NiO completely, and no other impurities are observed. Scanning electron microscope (SEM) was employed to investigate the morphology and microstructure of the NiO nanosheets/nanowires. Fig. 1b demonstrates a low-magnification SEM image of the NiO nanosheets/nanowires supported on the Ni foam, showing a 3D macro-porous structure without any macroscopical defects. Fig. 1c and d show different magnification SEM images of as-synthesized NiO nanosheets/nanowires. Obviously, the products exhibited NiO nanosheet arrays uniformly grew on the skeletons of the Ni foam as a secondary microstructure to form a 3D porous framework, which could make NiO ultrafine nanowires intercrossed grow with multiple directions on the nanosheets, exhibiting a unique hierarchical feature with reasonable intervals among adjoining nanostructures. Thus, the as-formed NiO nanosheets/nanowires are highly accessible to the electrolyte and engage in the reversible faradic reaction adequately due to the presence of convenient diffusion paths when used as an electrode for supercapacitors.

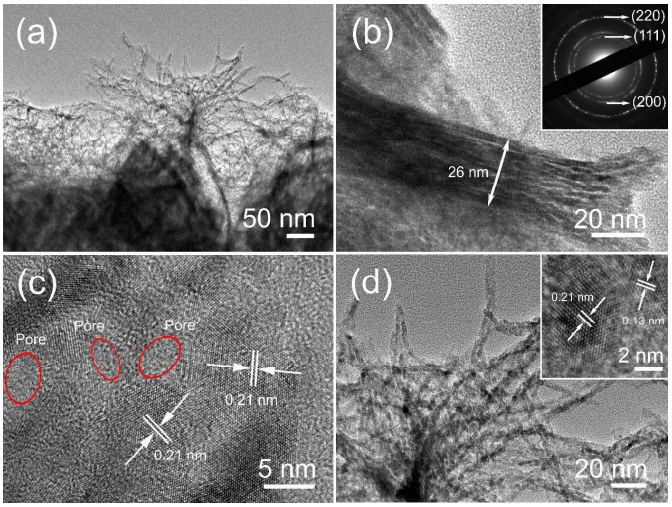

Fig. 2 (a) TEM image of the hierarchical NiO nanosheets/nanowires scraped off from the Ni foam. (b, c) TEM and HRTEM images of one segment of mesoporous NiO nanosheet. The inset in Fig.2b is the corresponding SAED image. (d) High-magnification TEM image of the ultrafine nanowires. The inset is the corresponding HRTEM image.

Further structural information about the hierarchical NiO nanosheets/nanowires was obtained from transmission electron microscope (TEM) image, as shown in Fig. 2a-d. Fig. 2a shows the TEM image of the NiO nanosheets/nanowires scraped off from the Ni foam. Noticeably, the NiO nanosheets were used as the backbone material, while the NiO ultrafine namowires were rooted on the nanosheets. Shown in Fig. 2b is one segment of the NiO nanosheet with a thickness of ~ 26 nm detached from the NiO nanosheets/nanowires. The corresponding selected area electron diffraction (SAED) pattern, shown in the inset of Fig. 2b, reveals these selected area electron diffraction rings can be well indexed by using the face-centered cubic with a lattice constant of a = 0.4177 nm, in agreement with the data in literature (JCPDS card No.: 65-5745). The first three diffraction rings (from the inside to the outside) are interpreted as (111), (200), and (220), reflections, respectively, for the NiO crystals within the hierarchical NiO nanosheets/nanowires. A high-resolution TEM image (HRTEM) of the nanosheet also demonstrated in Fig. 2c, revealing some visible lattice fringes with an equal interplanar distance of 0.21 nm, corresponding to the (200) planes of the NiO crystal. In addition, the nanosheets are porous, in which as-formed pores were related to the gas release during the calcination treatment, as shown in red ellipses of Fig. 2c. The high-magnification TEM image of the ultrafine nanowires, as shown in Fig. 2d, exhibits a diameter of ~ 2-4 nm. The corresponding HRTEM image (inset) reveals lattice fringes with interplane spacings of 0.21 and 0.13 nm, corresponding to the distance of the (200) and (311) planes, respectively, of the NiO crystal.

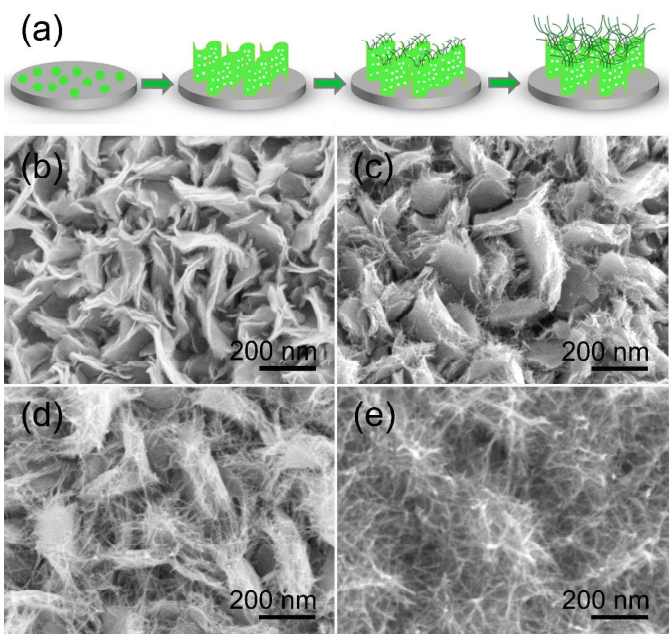

Fig. 3 (a) Schematic mechanism for the growth process of the hierarchical NiO nanosheets/nanowires with Ni foam as substrate. SEM images of the unique hierarchical microstructure with different reaction times: (b) 1 h, (c) 2 h, (d) 6 h, and (e) 12 h.

The porous feature of NiO nanosheets/nanowires is further confirmed by means of Brunauer-Emmett-Teller (BET, surface areas of 110.716 $m^2 g^{-1}$) and Barrett-Joyner-Halenda (BJH, average pore sizes of 6.8 nm) (Fig. S1). Such unique NiO nanosheets/nanowires with a higher specific surface area than that of the mesoporous NiO nanosheets (surface areas of 106.865 $m^2 g^{-1}$ and average pore sizes of 8.1 nm) have numerous transportation channels, which can facilitate the fast diffusion of electrolyte ions to the unique microstructure for efficient energy storage, ensuring exceptional pseudocapacitive properties for the NiO nanosheets/nanowires. The energy dispersive X-ray (EDX) spectrometer microanalysis of the hierarchical NiO nanosheets/nanowires was also investigated (Fig. S2). It was found that the unique hierarchical microstructure consist of only Ni and O elements except for the Cu peaks derived from Cu grid, further indicating the formation of pure NiO crystal.

To explore the formation mechanism of the as-synthesized NiO nanosheets/nanowires with Ni foam as substrate, we have carried out the reaction time dependent experiments at different reaction stages. Fig. 3a demonstrates the schematic mechanism for the growth process of the NiO nanosheets/nanowires on Ni foam, indicating the structural and morphological evolution from the nanoparticles to nanosheets with ultrafine nanowires. When putting the Ni foam into the autoclave, many NiO precursor nucleis appear on the surface of the Ni foam. After the initial 1 h reaction, nanosheet arrays based on the nucleis appeared and aligned, grown with a high density on the substrate (Fig. 3b). With the hydrothermal reaction time increasing to 2 h, the nanosheets turned into thicker ones along with many ultrafine and short nanowires appeared and rooted on the surface of the nanosheet arrays (Fig. 3c). Interestingly, with continuous extending reaction time, these nanowires became long and dense, exhibiting a perfect hierarchical microstructure with suitable room among adjoining nanounits to provide excellent capability in fast ion and electron transfer when as an electrode for pseudocapacitors (Fig. 3d). Further increasing the reaction time to 12 h, the nanowires got extremely dense and longer and cover the nanosheet arrays completely (Fig. 3e). This formation process seems to be an

analogous phenomenon in crystal growth processes observed in other material systems. [33-35]

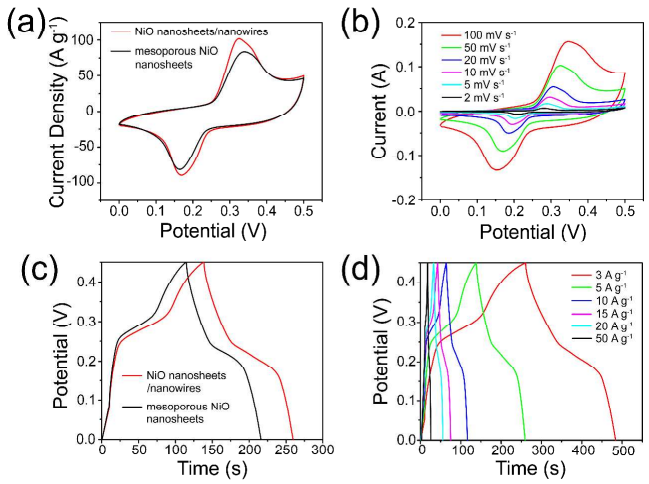

Fig. 4 (a) CV curves of the NiO nanosheets/nanowires and mesoporous NiO nanosheets at a scan rate of 50 mV s^{-1}. (b) CV curves of the NiO nanosheets/nanowires at different scan rates. (c) Galvanostatic charge-discharge curves of the NiO nanosheets/nanowires and mesoporous NiO nanosheets with a current density of 5 A g^{-1}. (d) Galvanostatic charge–discharge curves of the NiO nanosheets/nanowires at different current densities.

In order to investigate the pseudocapacitive properties of the unique hierarchical microstructure, the NiO nanosheets/nanowires on Ni foam were directly applied as an integrated electrode in a three-electrode configuration with 6 M KOH as the electrolyte. Fig. 4a shows the cyclic voltammetry (CV) curves of the NiO nanosheets/nanowires and mesoporous NiO nanosheets at a scan rate of 50 mV s^{-1}, both of the two curves reveal that the capacitive characteristics are different from those of electrochemical double-layer capacitors, which have an approximately rectangular and symmetric shape. A distinct pair of redox peaks during the cathodic and anodic sweeps were observed within the potential range from 0-0.5 V, demonstrating standard pseudocapacitive nature with fast charge-discharge processes, which could be attributed to the following reversible redox reaction: [36, 37]

$$NiO + OH^- \leftrightarrow NiOOH + e^-$$

It is obvious that the enclosed area of the NiO nanosheets/nanowires is larger than that of the NiO mesoporous nanosheets, indicating that the NiO nanosheets/nanowires delivered a higher specific capacitance. This could be attributed to great access of the electrolyte to the active surface of the NiO nanosheets/nanowires electrode materials. Further CV investigations of the NiO nanosheets/nanowires under different scan rates were then administered. Interestingly, with the scan rate increasing from 2 to 100 mV s^{-1}, the redox current increased (as shown in Fig. 4b). Also, the shape of the CV curves basically remains unchanged except for the oxidation and reduction peaks shifted toward higher and lower potentials, respectively, with a large potential separation, indicating outstanding electrochemical reversibility. Similar phenomenon was also observed in the mesoporous NiO nanosheets (Fig. S3).

Galvanostatic charge-discharge measurements were also carried out on the hierarchical microstructure at different current densities. Fig. 4c shows the charge-discharge curves of the NiO nanosheets/nanowires and mesoporous NiO nanosheets at a current density of 5 A g^{-1}. It can be seen that the charge curves are not strictly but approximately symmetric to their corresponding discharge counterparts, also indicating their good reversibility, which is consistent with the CV investigations. It is worthy noted that the specific capacitance of the NiO nanosheets/nanowires can reach 1349 F g^{-1}, which is significantly higher than that of the mesoporous NiO nanosheets (1130 F g^{-1}). Further galvanostatic CD investigations of the NiO nanosheets/nanowires and mesoporous NiO nanosheets between 0 and 0.45 V at different current densities are shown in Fig. 5d and S2. The superior pseudocapacitance of the NiO nanosheets/nanowires electrode were 1493, 1349, 1169, 1073, 1013 and 867 F g^{-1} at current densities of 3, 5, 10, 15, 20 and 50 A g^{-1}, respectively, which is higher than that of mesoporous NiO nanosheets (1250 F g^{-1} and 633 F g^{-1} at current densities of 3 A g^{-1} and 50 A g^{-1}, respectively). Importantly, these performance of the hierarchical microstructure is remarkable compared with the reported NiO based hierarchical microstructure, such as TiO_2/NiO core/shell nanorod arrays (~ 611 F g^{-1} at 2 A g^{-1}),[38] NiO/MnO_2 core/shell nanocomposites (~ 413.3 F g^{-1} at 1 A g^{-1}),[39] mesoporous NiO/C nanocomposites (~ 931 F g^{-1} at 2 A g^{-1}),[40] flowerlike NiO/reduced graphene oxide composites (~ 428 F g^{-1} at 0.38 A g^{-1}),[41] porous ZnO/NiO composite micropolyhedrons (~ 649 F g^{-1} at 5.8 A g^{-1}).[42] In addition, the Ni foam substrate may influence the pseudocapacitive properties, so we compared blank Ni foam with the NiO nanosheets/nanowires (Fig.S4) and found that the nickel foam's mass capacitance contribution on the results can be negligible.

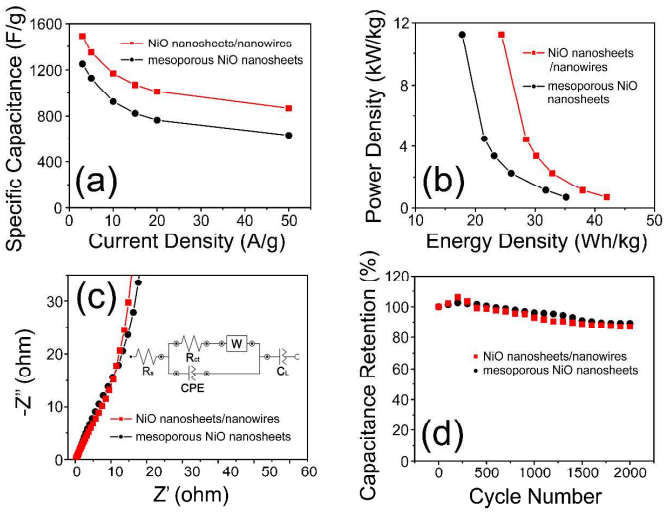

Fig. 5 (a) Specific capacitance at different current densities, (b) Ragone plot (power density vs. energy density), (c) EIS spectra comparison and (d) variation of specific capacitance with cycle number at a scan rate of 50 mV s^{-1} of the hierarchical NiO nanosheets/nanowires and mesoporous NiO nanosheets, respectively. The inset in Fig. 5c shows the equivalent fitting circuit of as-formed NiO electrodes.

Rate capability is a critical factor for evaluating the performance of the supercapacitors. A good supercapacitor is expected to provide high power at high rates. Shown in Fig. 5a is the variation of the specific capacitance of the NiO nanosheets/nanowires and mesoporous NiO nanosheets electrodes with the increase in the current density. As can be seen, the NiO nanosheets/nanowires electrode preserved 58% of its specific capacitance (from 1493 to 867 F g^{-1}) with the current increasing from 3 to 50 A g^{-1}, which is splendid than that (50.8%) of the mesoporous NiO nanosheets, indicating that the NiO nanosheets/nanowires electrode is more suitable when used in high power application. Power density and energy density are two key factors for assessing the performance of

the supercapacitors. Fig. 5b shows the Ragone plot for the two electrodes at the potential window of 0-0.45 V. At a power density of 675 W kg^{-1}, the NiO nanosheets/nanowires electrode materials deliver an energy density as high as 41.98 Wh kg^{-1}, which is larger than that of the mesoporous NiO nanosheets electrode materials (35.16 Wh kg^{-1}). Significantly, the energy density of the prepared electrode from the NiO nanosheets/nanowires is higher than those of the reported binder-free nanostructured NiO electrodes, such as NiO nanoflake (35.59 Wh kg^{-1}),[43] NiO nanoplatelet arrays (39.03 Wh kg^{-1}),[44] NiO nanosheet arrays (18.96 Wh kg^{-1}),[45] NiO nanotube arrays (15 Wh kg^{-1}) [46] and NiO nanostructures (18.02 Wh kg^{-1}).[47] In addition, electrochemical impedance spectroscopy (EIS) was also employed to characterize the hierarchical microstructure electrodes, as shown in Fig. 5c. The impedance curves are similar in form, with an unclear arc in the high-frequency region and a spike at lower frequencies, seeming to be an analogous form to other reported curves from NiO material.[48] The inset of Figure 2c shows the equivalent fitting circuit of as-formed NiO electrodes. The equivalent series resistance (R_s) value of the NiO nanosheets/nanowires was only 0.25 Ω, which was lower than that (0.40 Ω) of the mesoporous NiO nanosheets. Moreover, the calculated charge-transfer resistances (R_{ct}) for the NiO nanosheets/nanowires extracted at a high frequency range was estimated to be ~ 0.0146 Ω, in contrast to ~ 0.0833 Ω for the mesoporous NiO nanosheet electrode, indicating a superior conductivity of the NiO nanosheets/nanowires hierarchical microstructures due to that the ultrafine NiO nanowires have more electroactive sites and provide short paths for ion and electron transport. Cycling performance is another key factor in determining the supercapacitors for many practical applications. In this study, a long-term cycle stability of the as-synthesized products as an electrode material was evaluated by repeating the CV test at a scan rate of 50 mV s^{-1} for 2000 cycles, as shown in Fig. 5d. It can be clearly seen that the specific capacitance retention of such two electrode materials gradually increases firstly and then slightly decreases. This indicates that there is an activation process of the electrode at the beginning period of the CV cycling test. During this process, the electrode will be activated adequately through the intercalation and de-intercalation of ions through some circulations, resulting in the increase of active points inside the electrode materials. The overall capacitance loss of the NiO nanosheets/nanowires is as low as 13% after 2000 cycles, while the overall capacitance loss of the mesoporous NiO nanosheets is 11% after 2000 cycles. The above results demonstrate that both the NiO nanosheets/nanowires and mesoporous NiO nanosheets electrode are highly stable during a cycling test.

The pretty good pseudocapacitance performances can be attributed to the unique morphology and structure of the NiO nanosheets/nanowires on Ni foam. Firstly, the hierarchical microstructure directly grown on the conductive Ni foam can insure a good mechanical adhesion and electrical connection to the current collector; designing additive/binder-free electrode microstructures also could avoid 'dead' volume, which would have an opposite effect in the improvement of pseudocapacitive performance. Secondly, the mesoporous nanosheets and ultrafine nanowires can greatly increase electroactive sites and make them fully get access to the electrolyte. Thirdly, the reasonable room among adjoining mesoporous nanosheets or ultrafine nanowires allows for easy diffusion of the electrolyte into the inner region of the electrode. Thus, the as-formed microstructure can participate in the reversible faradic reaction adequately and deliver exceptional pseudocapacitive properties.

Conclusions

In summary, hierarchical NiO ultrafine nanowires grown on mesoporous NiO nanosheets with Ni foam as substrate was farbricated by a facile, effective, and low-cost hydrothermal method for high-performance pseudocapacitors. The hierarchical NiO nanosheets/nanowires as electrode material delivered ultrahigh specific capacitance of 1349 F g^{-1} at the current density of 5 A g^{-1}, which is superior to 1130 F g^{-1} of the mesoporous NiO nanosheet arrays at the same current density. In addition, the unique hierarchical electrode microstructure also exhibited a good rate performance (~58% retention of the initial capacitance from 3 A g^{-1} to 50 A g^{-1}) and a high electrochemical stability (~87% retention after 2000 cycles). The outstanding electrochemical performance can make the hierarchical NiO nanosheets/nanowires to be one of the perspective electrode materials for electrochemical energy storage applications.

Acknowledgements

This work was financially supported by the National Natural Science Foundation of China (Grant Nos. 21171035 and 51302035), the Key Grant Project of Chinese Ministry of Education (Grant No. 313015), the PhD Programs Foundation of the Ministry of Education of China (Grant Nos. 20110075110008 and 20130075120001), the National 863 Program of China (Grant No. 2013AA031903), the Science and Technology Commission of Shanghai Municipality (Grant No. 13ZR1451200), the Fundamental Research Funds for the Central Universities, the Program Innovative Research Team in University (IRT1221), the Shanghai Leading Academic Discipline Project (Grant No. B603), and the Program of Introducing Talents of Discipline to Universities (No. 111-2-04).

Notes and references

a State Key Laboratory for Modification of Chemical Fibers and Polymer Materials, College of Materials Science and Engineering, Donghua University, Shanghai 201620, China.
b School of material engineering, Shanghai university of engineering science, Shanghai 201620, China
c Center of Super-Diamond and Advanced Films (COSDAF), Department of Physics and Materials Science, City University of Hong Kong, Hong Kong.

E-mail: hu.junqing@dhu.edu.cn, rjzou@dhu.edu.cn.

Electronic Supplementary Information (ESI) available. See DOI: 10.1039/b000000x/

1 P. Simon and Y. Gogotsi, *Nat. Mater.*, 2008, **7**, 845.
2 G. P. Wang, L. Zhang and J. J. Zhang, *Chem. Soc. Rev.*, 2012, **41**, 797.
3 C. Liu, F. Li, L. P. Ma and H. M. Cheng, Adv. Mater., 2010, **22**, 28.
4 M. Kaempgen, C. K. Chan, J. Ma, Y. Cui and G. Gruner, *Nano Lett.,* 2009, **9**, 1872.
5 W. Sugimoto, H. Iwata, Y. Yasunaga, Y. Murakami and Y. Takasu, *Angew. Chem., Int. Ed*. 2003, **42**, 4092.
6 H. B. Li, M. H. Yu, F. X. Wang, P. Liu, Y. Liang, J. Xiao, C. X. Wang and Y. X. Tong , G. W. Yang, *Nat. Comm*., 2013, **4**, 1894.
7 G. Lee, Y. W. Cheng, C. V. Varanasi and J. Liu, *J. Phys. Chem. C*, 2014, **118**, 2281.

8 S. K. Meher, P. Justin and G. R. Rao, *ACS Appl. Mater. Interfaces*, 2011, **3**, 2063.
9 C. W. Kung, H. W. Chen, C. Y. Lin and R. Vittal, *J. Power Sources*, 2012, **214**, 91.
10 C. W Cheng and H. J. Fan, *Nano Today*, 2012, **7**, 327.
11 L. Wang, Z. H. Dong, Z. G. Wang, F. X. Zhang and J. Jin, *Adv. Funct. Mater.*, 2013, **23**, 2758.
12 C, Mondal, M. Ganguly, P. K. Manna, S. M. Yusuf and T. Pal, *Langmuir*, 2013, **29**, 9179.
13 B. Wang, J. S. Chen, Z. Y. Wang, S. Madhavi and X. W. Lou, *Adv. Energy. Mater.*, 2012, **2**, 1188.
14 S. I. Kim, J. S. Lee, H. J. Ahn, H. K. Song and J. H. Jang, *ACS Appl. Mater. Interfaces*, 2013, **5**, 1596.
15 W. Wen, J. M. Wu and M. H. Cao, *Nano Energy*, 2013, **2**, 1383.
16 Q. Lu, M. W. Lattanzi, Y. P. Chen, X. M. Kou, W. F. Li, X. Fan, K. M. Unruh, J. G. Chen and J. Q. Xiao, *Angew. Chem. Int. Ed.*, 2011, **50**, 6847.
17 Z. H. Yang, F. F. Xu, W. X. Zhang, Z. H. Mei, B. Pei and X. Zhu, *J. Power Sources*, 2014, **246**, 24.
18 S. L. Xiong, C. Z. Yuan, X. G. Zhang and Y. T. Qian, *CrystEngComm*, 2011, **13**, 626.
19 X. W. Li, S. L. Xiong, J. F. Li, J. Bai and Y. T. Qian, *J. Mater. Chem.*, 2012, **22**, 14276.
20 W. J. Zhou, X. H. Cao, Z. Y. Zeng, W. H. Shi, Y. Y. Zhu, Q. Y. Yan, H. Liu, J. Y. Wang and H. Zhang, *Energy Environ. Sci.*, 2013, **6**, 2216.
21 J. P. Liu, J. Jiang, C. W. Cheng, H. X. Li, J. X. Zhang, H. Gong and H. J. Fan, *Adv. Mater.*, 2011, **23**, 2076.
22 R. B. Rakhi, W. Chen, D. K. Cha and H. N. Alshareef, *Nano Lett.*, 2012, **12**, 2559.
23 A. L. M. Reddy, M. M. Shaijumon, S. R. Gowda and P. M. Ajayan, *Nano Lett.*, 2009, **9**, 1002.
24 H. Jiang, J. Ma and C. Z. Li, *Chem. Commun.,* 2012, **48**, 4465.
25 W. Y. Li, Q. Liu, Y. G. Sun, J. Q. Sun, R. J. Zou, G. Li, X. H. Hu, G. S. Song, G. X. Ma, J. M. Yang, Z. G. Chen and J. Q. Hu, *J. Mater. Chem.*, 2012, **22**, 14864.
26 L. F. Shen, Q. Che, H. S. Li and X. G. Zhang, *Adv. Funct. Mater.*, 2013, DOI: 10.1002/adfm.201303138.
27 L. F. Chen, X. D. Zhang, H. W. Liang, M. G. Kong, Q. F. Guan, P. Chen, Z. Y. Wu and S. H. Yu, *ACS Nano*, 2012, **6**, 7092.
28 M. C. Liu, L. B. Kong, C. Lu, X. M. Li, Y. C. Luo and L. Kang, *Mater. Lett.*, 2013, **94**, 197.
29 F. L. Zheng, G. R. Li, Y. N. Ou, Z. L. Wang, C. Y. Su and Y. X. Tong, *Chem. Commun.*, 2010, **46**, 5021.
30 L. F. Chen, Z. H. Huang, H. W. Liang, Q. F. Guan and S. H. Yu, *Adv. Mater.*, 2013, **25**, 4746.
31 M. H. Yu, Y. X. Zeng, C. Zhang, X. H. Lu, C. H. Zeng, C. Z. Yao, Y. Y. Yang and Y. X. Tong, *Nanoscale*, 2013, **5**, 10806.
32 X. H. Xia, J. P. Tu, Y. Q. Zhang, X. L. Wang, C. D. Gu, X. B. Zhao and H. J. Fan, *ACS Nano*, 2012, **6**, 5531.
33 Q. Yang, Z. Y. Lu, Z. Chang, W. Zhu, J. Q. Sun, J. F. Liu, X. M. Sun and X. Duan, *RSC Adv.*, 2012, **2**, 1663.
34 W. Zhu, Z. Y. Lu, G. X. Zhang, X. D. Lei, Z. Chang, J. F. Liu and X. M. Sun, *J. Mater. Chem. A*, 2013, **1**, 8327.
35 X. Y. Liu, Y. Q. Zhang, X. H. Xia, S. J. Shi, Y. Lu, X. L. Wang, C. D. Gu and J. P. Tu, *J. Power Sources*, 2013, **239**, 157.
36 X. Y. Yan, X. L. Tong, J. Wang, C. W. Gong, M. G. Z and L. P. Liang, *Mater. Lett.*, 2013, **95**, 1.
37 B. Ren, M. Q. Fan, Q. Liu, J. Wang, D. L. Song and X. F. Bai, *Electrochim. Acta.* 2013, **92**, 197.
38 J. B. Wu, R. Q. Guo, X. H. Huang and Y. Lin, *J. Power Sources*, 2013, **243**, 317.
39 B. J. Zhang, W. Y. Li, J. Q. Sun, G. J. He, R. J. Zou, J. Q. Hu and Z. G. Chen, *Mater. Lett.*, 2014, **114**, 40.
40 K. B. Xu, R. J. Zou, W. Y. Li, Q. Liu, T. Wang, J. M. Yang, Z. G. Chen and J. Q. Hu, *New J. Chem.*, 2013, 37, 4031.
41 W. Li, Y. F. Bu, H. L Jin, J. Wang, W. M. Zhang, S. Wang and J. C. Wang, *Energ. Fuel,* 2013, 27, 6304.
42 H. Pang, Y. H. Ma, G. C Li, J. Chen, J. S. Zhang, H. H. Zheng and W. M. Dua, *Dalton Trans.*, 2012, 41, 13284.
43 D. T. Dam, X. Wang and J. M. Lee. *Nano Energy*, 2013, 2, 1303.
44 C. Z. Yuan, J. Y. Li, L. R. Hou, L. Yang, L. F Shen and X. G. Zhang. *Electrochim. Acta.,* 2012, 78, 532.
45 M. Huang, F. Li, J. Y. Ji, Y. X. Zhang, X. L. Zhao and X. Gao. *CrystEngComm*, 2014, 16, 2878.
46 F. Cao, G.X. Pan, X. H. Xia, P. S. Tang and H. F. Chen. *J. Power Sources*, 2014, DOI: 10.1016/j.jpowsour.2014.04.103.
47 F. I. Dar, K. R. Moonooswamy and M. E. Souni. *Nanoscale Res. Lett.,* 2013, 8, 363.
48 D. D. Han, P. C. Xu, X. Y Jing, J. Wang, P. P. Yang, Q. H. Shen, J. Y. Liu, D. L. Song, Z. Gao, M. L. Zhang. *J. Power Sources*, 2013, 235, 45.